25th ABCM International Congress of Mechanical Engineering
October 20-25, 2019, Uberlândia, MG, Brazil

COB-2019-1353
RESIDUAL STRESSES DURING AND AFTER WELDING AUTOGENOUS PROCESSES AND WITH MATERIAL DEPOSITION

Tarcila Rocha França
Douglas Silva Marques Serrati
Federal University of Uberlândia
tarcilarochafranca@gmail.com
douglasserrati@gmail.com

Douglas Bezerra de Araújo
Federal University of Uberlândia
dbaraujo@ufu.br

Louriel Oliveira Vilarinho
Federal University of Uberlândia
vilarinho@ufu.br

Abstract. *The objective of this work was to compare, through finite element analysis, residual stresses during and after two processes, welding autogenous and with material deposition. The purpose was to quantify the differences obtained in results between these two process, in order to offer knowledge enough to ponder which of this analysis should be used. To get the expected results, thermal and structural analyses were done, whereupon it is possible to associate informations about temperature, shrinkage, distortions and residual stresses during welding process.*

Keywords: *welding, residual stresses, simulation, autogenous*

1. INTRODUCTION

Arc welding processes are characterizes by the imposition of an intense heat source that will melt and bond the materials being welded. Because it is a localized source of heat, non-uniform plastic dilations, contractions and deformations will occur, causing deformations and residual stresses. These stresses are usually tensile in the cord and close to it and compressive in the rest of the material. The tensile stresses can damage the final design of the structure that has been welded, which can propagate catastrophic cracks in the structure. In addition, distortions of the welded material may impair the proper functioning of the structure or in some cases even lose the structure due to difficulties in the assembly. In this way, it becomes important to study how the distortions occur and how residual stresses are formed during the welding process and it is possible consequences. This work shows through the computational simulation using the finite element technique, the evolution of stresses during and after welding. In addition, a comparison of the evolution of these stresses in autogenous welding processes (without addition of matter) and welding with deposition of material is done. The results showed that the distortions that occur in the plates are very different when using autogenous process and process with material deposition.

2. CASE STUDY

In order understand the development of stresses along the plate during and after the autogenous welding processes and with material deposition, the finite element technique was used. The simulation was composed for a heat source of the Gaussian type on a low carbon steel plate with the dimensions of 200 x 100 x 3.2 mm. For welding process with deposition, the weld bead geometry is show in Fig.1. The stresses generated by the welding process are thermo-structural analysis, the thermal and mechanical properties are temperature-dependent used by Miettinen (1997) and Tsirkas et al. (2003). In addition, for the process with material deposition, the “birth and death” technique was used. This technique consists of a numerical model that to be birth previously dead elements. In this work, the “birth and death” technique was used for to make appear the weld bead during welding processes.

For all cases described above, a transient analysis was used with travel speed of 5 mm/s, an effective welding power of 1200 W and without external restrictions.

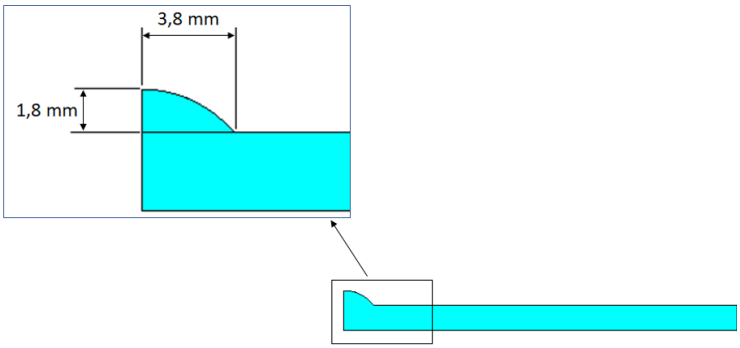

Figure 1. Weld bead geometry

The thermal field is governed by the heat conduction equation given by:

$$\frac{\partial}{\partial x}\left(k(T)\frac{\partial T}{\partial x}\right)+\frac{\partial}{\partial y}\left(k(T)\frac{\partial T}{\partial y}\right)+\frac{\partial}{\partial z}\left(k(T)\frac{\partial T}{\partial z}\right)+Q_v=\rho(T)C_p(T)\frac{\partial T}{\partial t} \quad (1)$$

where, T is the temperature, $k(T)$ is the thermal conductivity, $\rho(T)$ is the specific mass, $C_p(T)$ is the specific heat and Qv is the rate at which energy is generated per unit volume of the medium (in this study, Qv is null). The thermodynamic boyndary conditions on the external surfaces of the solid comprise heat transfer for convection and radiation. The heat flow density for convection (q_c) is guaranteed by Newton's law. Newton's law of cooling states that the rate of heat loss of a body is directly proportional to the difference in the temperatures between the body and its surroundings temperature, and is given by:

$$q_c = h_c(T - T_0) \quad (2)$$

where T is the temperature of the external surface, T_0 is the temperature of gas or liquid and h_c is the coefficient of convective heat transfer. The convection coefficient of the surface depends on many factors. Some authors, such as SORENCE, 1999; TENG et al., 2001 and GERY, LONG, MAROPOULOS, 2005 have proposed to use values of convection coefficient from 15 to 25 W / m^{2}K. In this work, the value of 15 W / m^{2}K was used. The radiation heat transfer (q_r) is governed by Stefan-Boltzmann's law, given by:

$$q_r = \varepsilon_r \sigma_r (T^4 - T_0^4) \quad (3)$$

where, ε_r is the emissivity of the material surface and σ_r is the Stefan–Boltzman constant (5.67×10^{-8} W·m^{-2}·K^{-4}). The value of the emissivity depends on the temperature in the welding process, however, in this study, this value was invariable, with a value of 0.80.

The heat of the welding arc was modeled by a traveling two-dimensional distribution of a heat source with a Gaussian distribution (Fig. 2). Therefore, the heat flux distribution on the surface of the solid is related to the radial position r (whose origin is the arc center), given by Eagar and Tsai (1983):

$$q_r = \frac{\eta U i}{2\pi\sigma^2} e^{-\left(\frac{r^2}{2\sigma^2}\right)} \quad (4)$$

where, q(r) is the surface flux at radius r, η is the thermal efficiency arc welding coefficient, U is the voltage, I is the current and σ is the radial distance from the center. In this study, the value for a σ was equal to 0,0015 m.

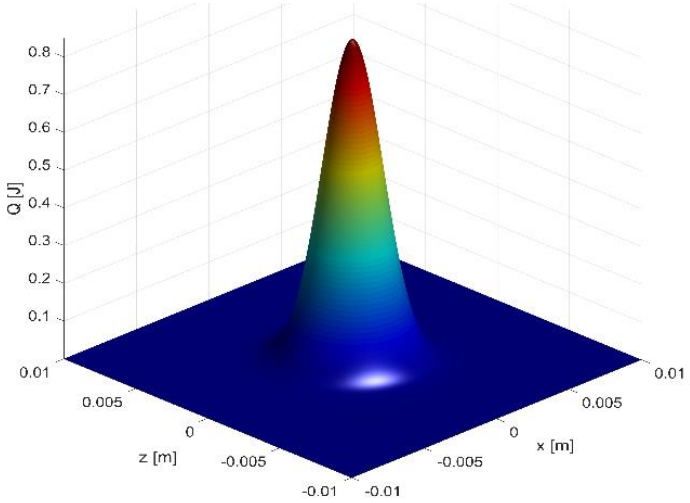

Figure 2. Gaussian distribution heat source for σ equal 0,0015m

2.1 Mechanical Analyses

In the mechanical analyses model used loading input the temperature history of thermal analysis. The total strain rate is decomposed into three components, as follows:

$$\varepsilon = \varepsilon^{e} + \varepsilon^{p} + \varepsilon^{th} \tag{5}$$

where, ε^{e}, $\varepsilon^{p}$and ε^{th} are elastic, plastic and thermal strain rate respectively. The elastic strain was modeled using the isotropic Hooke's law with temperature-dependent Young's modulus and Poisson's ratio. The plasticity strain was modeled using the perfectly plastic model temperature-dependent, that is, the effect of work hardening was neglected. The thermal strain is calculated by using temperature-dependent coefficient of thermal expansion.

2.2 Structural Boundary Condition e Finite Element

For structural boundary conditions are given as displacement at x equal to zero (dx = 0) in the plane of symmetry of the material, displacement at point A is equal to zero in the three directions (dx = dy = dz = 0) allowing rotation and displacement at point B equals zero in the y direction (dy = 0) (Fig. 3). These conditions are only for the convergence of the structural analysis do not interfere in the results of the problem.

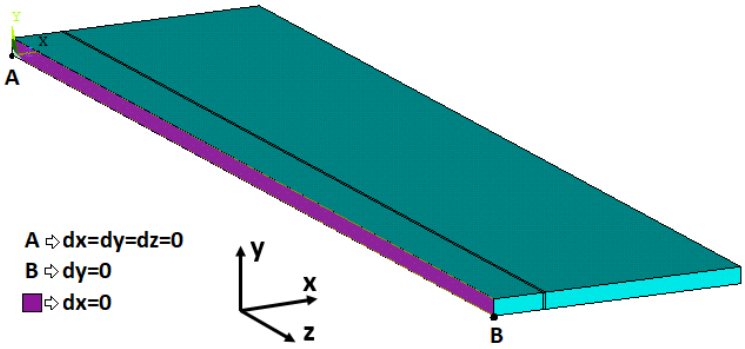

Figure 3. Structural boundary conditions

For the thermal analysis of the solid, the SOLID90 element with 20 nodes per element with a single degree of freedom, which is the temperature, was used. And for the thermal analysis of the surface with the natural convection and radiation the element SURF152 was used. This element is coupled to the outer surfaces of the solid elements and an extra node. For the structural analysis, the element SOLID186, which has the same characteristics as SOLID90, was

used, with degree of freedom of translation in the x, y and z directions. This element also has the capacity of plasticity and large deformations.

In this work, a structured mesh with a size of 0,5 mm was used in the region of the weld bead (0<x<0.01 m), and a mesh with size of 1 mm in the distal region between 0.0105 m and 0.05 m. And between the two regions was used an unstructured mesh of size of 0.5 mm.

3. RESULTS AND DISCUSSIONS

3.1 Thermal Analysis

The first results were the thermal analyzes of the autogenous processes and with material deposition processes. The Fig. 4 shows the temperature distribution over the entire plate for the time equal to 20 s. The maximum temperature was limited to 1500 °C considering the melting temperature of the material. Now, comparing the autogenous processes and the processes with material deposition can be observed by Fig. 5, that the depth of fusion zone in the autogenous process is greater, since it has less material to be heated. It is also important to note that the higher temperature levels are above the upper sheet line for the material deposition process (Fig. 5b). This feature may be very important in structural analysis.

The "Birth and death" technique was used in both thermal and structural analysis. In the thermal analysis, a technique was used to activate the dead elements previously in front of the Gaussian heat source (Fig.5b), because it is not possible to apply heat to the elements due to their almost zero thermal conductivity. This causes the temperature to rise to very extreme values by diverting the solution from the problem.

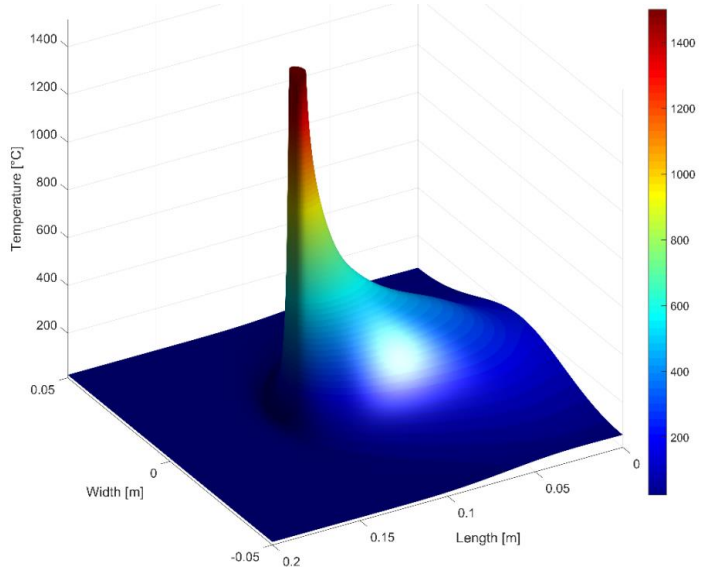

Figure 4. Isotherms during welding processes

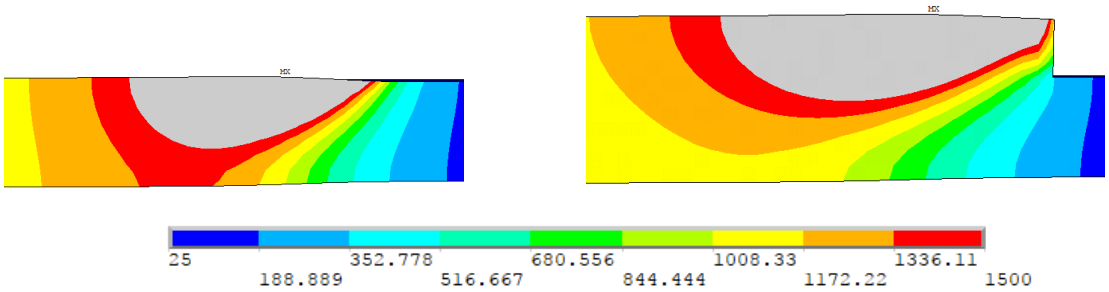

(a) (b)

Figure 5. Fusion zone and neighboring isotherms (a) autogenous process, (b) process with material deposition

3.2 Structural Analysis

The obtained structural results were the shrinkage, distortions and residual stresses for the autogenous processes and processes with material deposition.

3.2.1 Shrinkage and distortions

The two most studied cases of shrinkage and distortions are the transverse shrinkage and the displacement of the plate in the y direction, which are the bending and angular distortions. For the same effective power, one can see the transversal shrinkage for the autogenous processes and for the processes with material deposition in the Fig. 6. The Fig. 7 shows with more details the transverse shrinkage for x=0.01 m and x=0.05 m for both cases. It is possible to observe that there are no major differences between the autogenous processes and the processes with material deposition. In addition, the transverse shrinkage decreases with the distancing of the weld bead line.

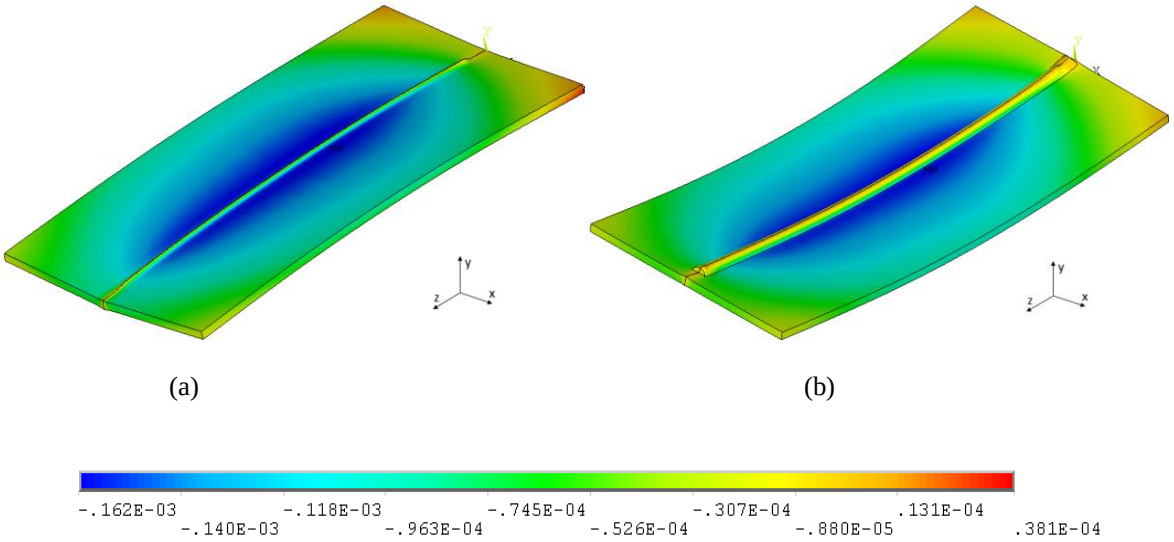

Figure 6 – Transverse shrinkage (a) autogenous process, (b) process with material deposition

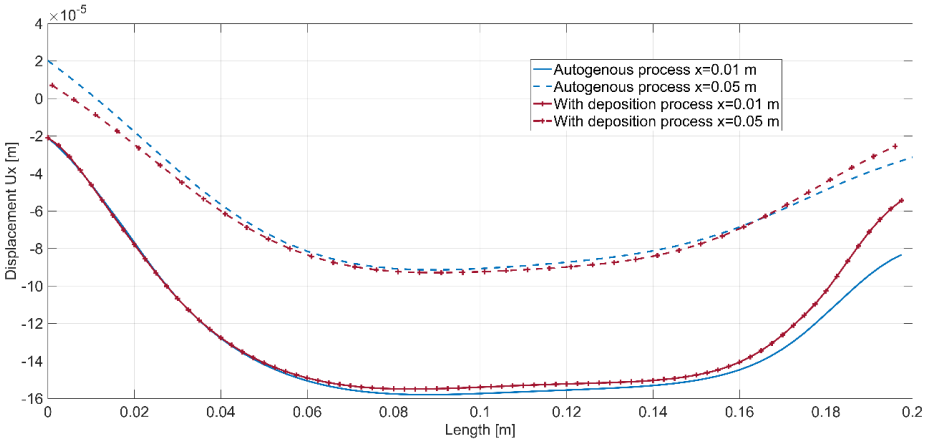

Figure 7 – Transverse shrinkage for x=0.01 m and x=0.05 m

There are two situations for y displacement, bending and angular distortion. The first the longitudinal ends move relative to the center of the plate. This can occur both positively and negatively. These two situations were evidenced in the autogenous processes and with deposition of material. The bending of the autogenous process showed a displacement y of the center of the sheet above the ends while the process with deposition showed a displacement y of the center of the sheet below the ends. These two situations are shown through Fig. 8, for x=0.01 m and x=0.05 m of distance from center. Angular distortion, on the other hand, shows a displacement of the transverse ends of the plate with respect to the center of the plate. The Fig. 9 shows the angular distortion of the autogenous processes and with

deposition of material. The autogenous process presents a greater angular distortion in comparison to the process with deposition.

The combination of the two types of distortions mentioned above for each process occurs a variation of the geometry of the plate as shown in Fig. 10. The autogenous process causes the sheet to have a "cell" appearance while in the deposition process the sheet has a concave appearance.

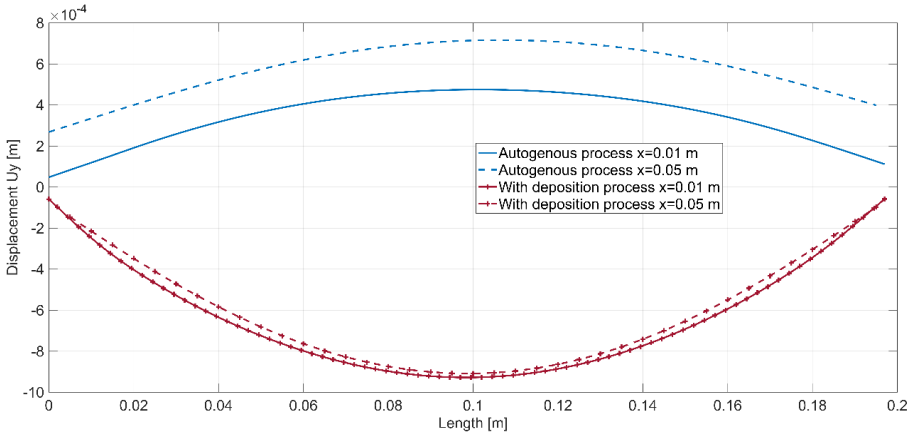

Figure 8 – Bending distortion after welding process for autogenous process, process with material deposition for x equal 0.01 m and 0.05 m

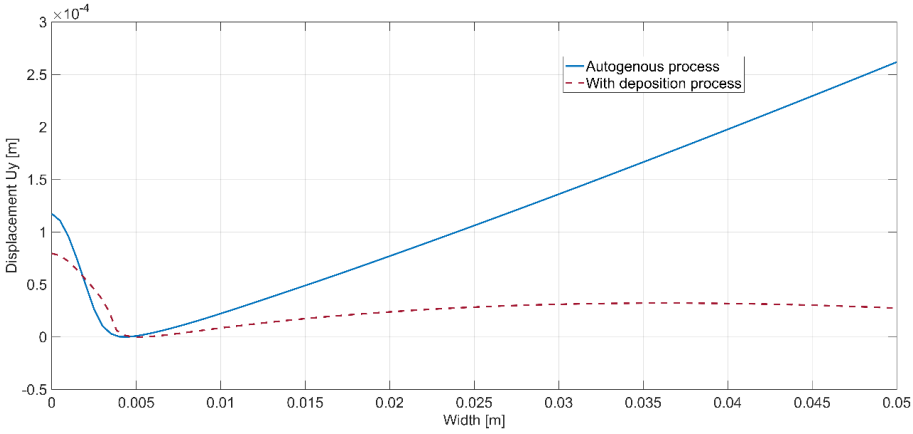

Figure 9 – Relative angular distortion for z=0.1 m

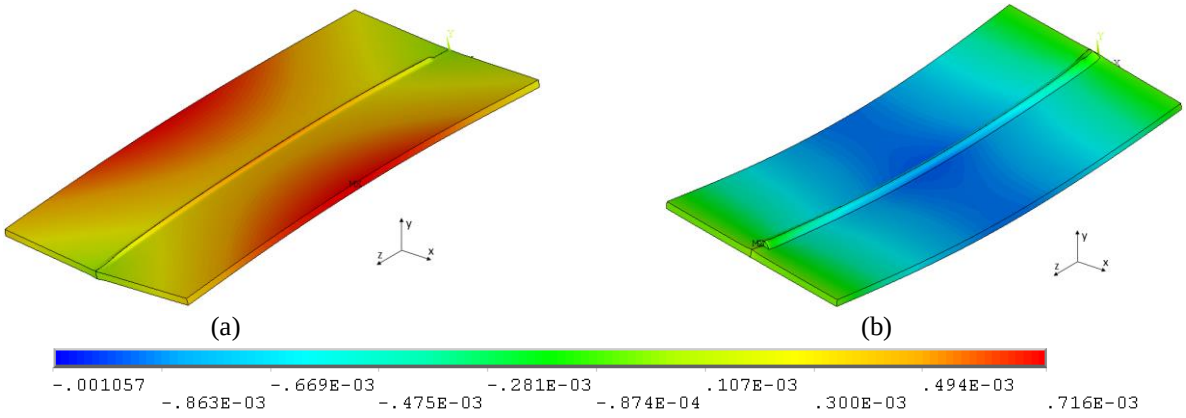

Figure 10 – Displacement in the y direction (a) autogenous process, (b) process with material deposition

3.2.2 Residual Stresses

Residual stresses are elastic stresses remaining in a body without the existence of external loads or temperature gradients. Every residual stress system is in equilibrium and the sum of the resulting forces is zero. To solve the structural analysis, it was necessary first the thermal solution that will serve as a boundary condition together with the expansion of the material.

The first results analyzed were the transversal stresses. These are stresses perpendicular to the welding direction which in this work is the x direction. The distribution of these stresses along the plate can be seen in Fig. 11. The Fig. 11 (a) which represents the transverse stresses in the autogenous process and Fig. 11 (b) which represents the transverse stresses in the material deposition process. Comparing the two cases it is possible to verify that the presence of the weld cord increases the value of the tensile transverse stresses near the cord. In addition, tensile stresses occur in the central region of the plate with larger values near the ends and the compressive stresses occur at the ends of the plate for both the autogenous process and the process with material deposition. Are these situations best evidenced in Fig. 12 (3D).

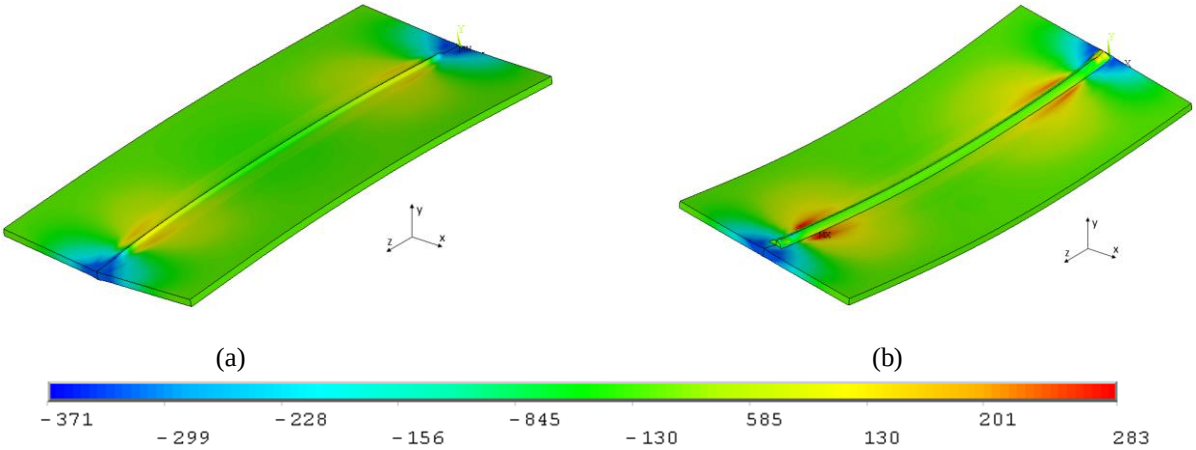

Figure 11– Transverse residual stresses after welding processes (t=20 s) (a) autogenous process, (b) process with material deposition [MPa]

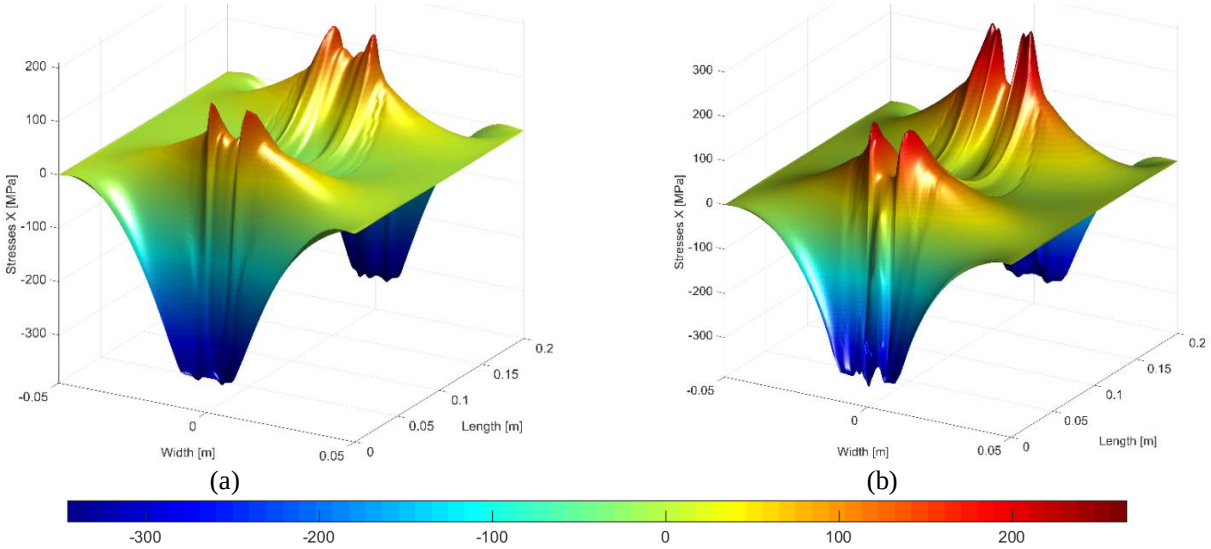

Figure 12 – Transverse residual stresses 3D of the surface plate after welding processes (t=20 s) (a) autogenous process, (b) process with material deposition [MPa]

Now, the distribution of the transverse stresses on the surface of the sheet during the welding process, in other words, t = 20s can be seen in the Figures. These results show that there is a very particular region that is region ahead of the heat source. This region presents high compressive stress values. In addition, the levels of tensile stresses after

passage of the heat source increase with its distance, that is, with the cooling of the region. This behavior occurs due to the properties of the metallic materials.

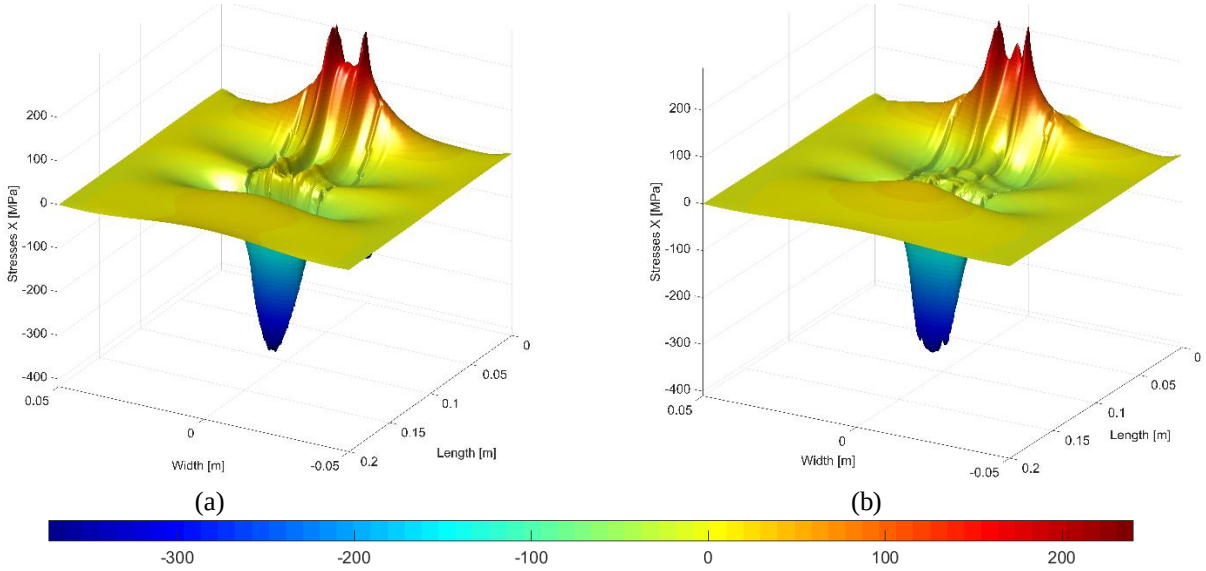

Figure 13 – Transverse residual stresses 3D of the surface plate during welding processes (t=20 s) (a) autogenous process, (b) process with material deposition [MPa]

Longitudinal residual stresses occur along the welding direction; in this case it is in the Z direction. The distribution of these stresses after the welding process and with the plate at room temperature can be seen in Fig.14 and the 3D distribution on the upper surface of the plate is shown in Fig. 15.

The tensile longitudinal stresses occur in the region of the weld bead and close to it, reaching up to almost two and a half times its width. After this region, the transition between traction and compression begins and after the compression region begins to reach the end of the sheet width.

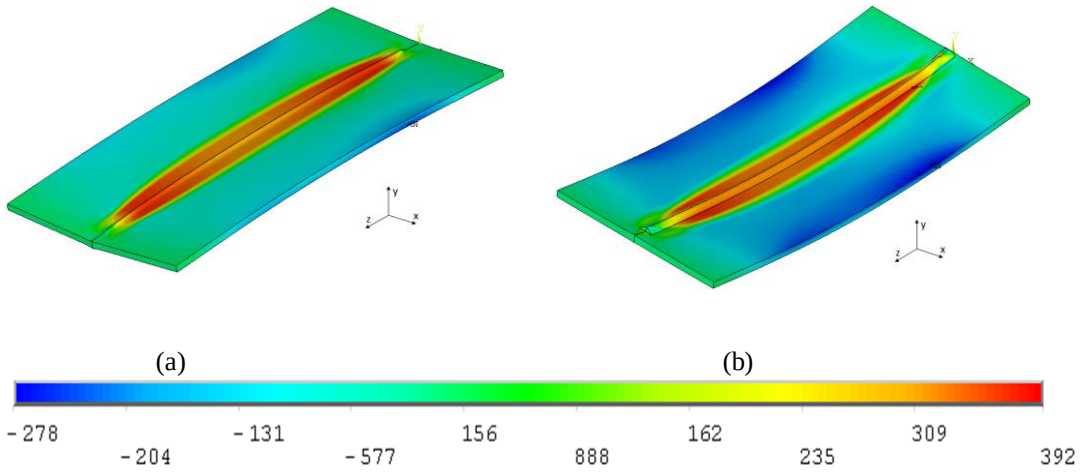

Figure 14- Longitudinal residual stresses (a) autogenous process, (b) process with material deposition [MPa]

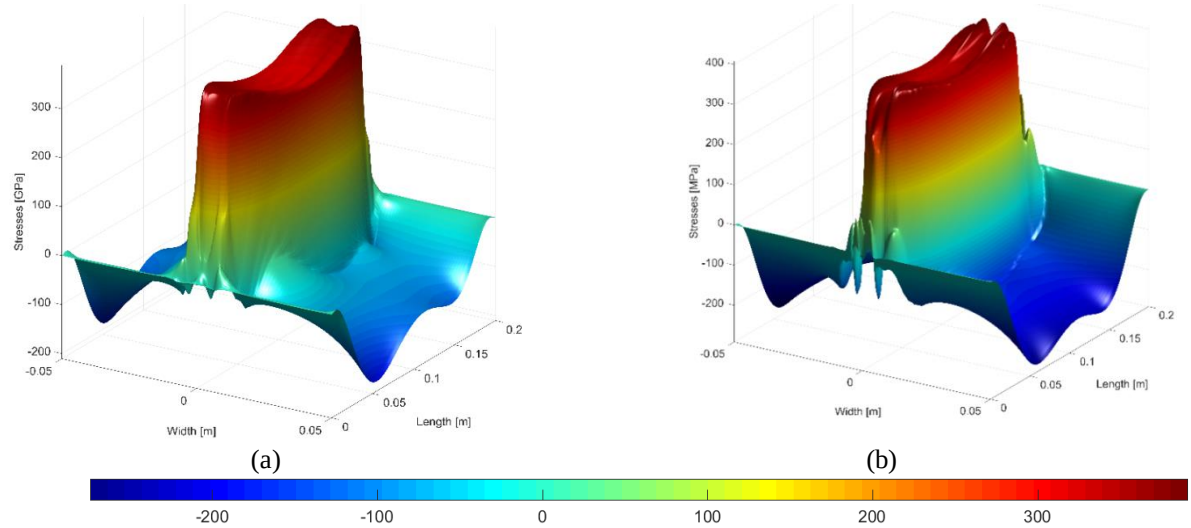

Figure 15. Longitudinal residual stresses 3D of the surface plate after welding process (a) autogenous process, (b) process with material deposition [MPa]

Comparing the autogenous process with the deposited process, the second presents values of longitudinal stresses greater in the transition of the weld bead with the plate, mainly in the longitudinal ends of the plate as shown in Fig. 15. In addition, in the central region of the weld bead, that is, for x = 0 the two cases do not differ much, only for regions farther from the cord (region of compressive stresses) that the difference is more pronounced as shown in Fig. 16 and Fig. 17.

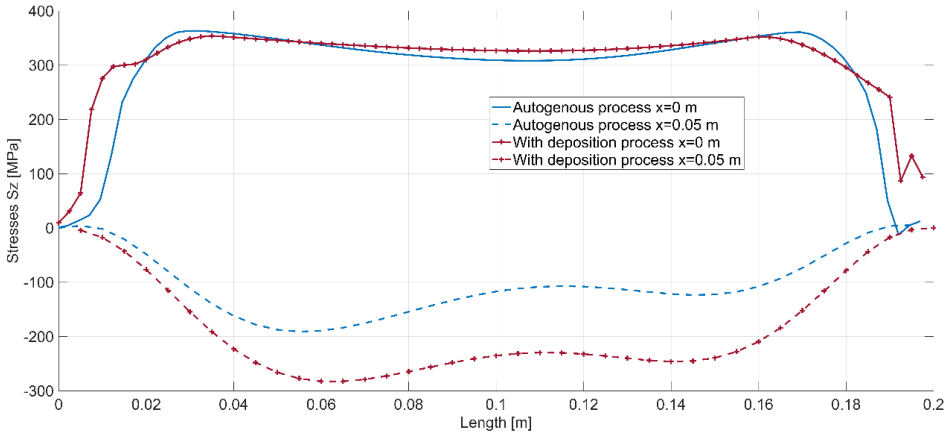

Figure 16 – Longitudinal stresses Sz for t=300 s

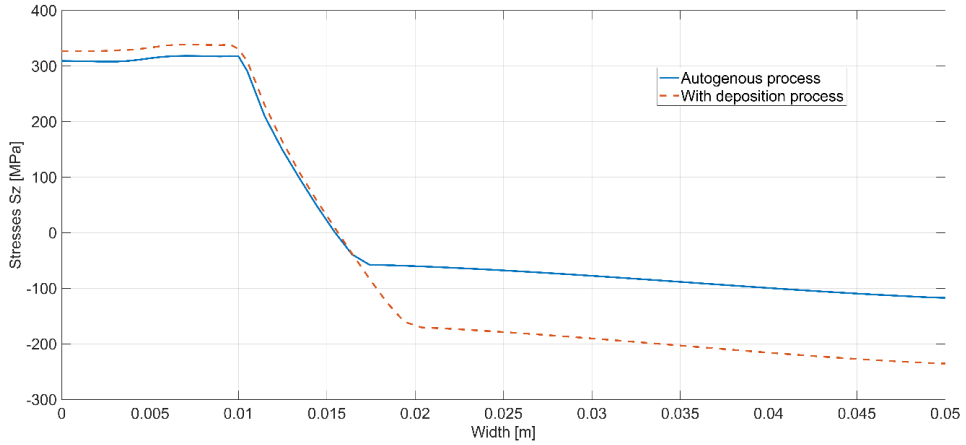

Figure 17 – Longitudinal stresses for z=0.1 m

Now, the longitudinal stresses during the welding process have different characteristics in comparison during the welding process and the end of the welding processes. The Fig.18 shows the distribution of the longitudinal stresses in the region of the weld bead for the time equal to 20 s. It is possible to observe that in front of the heat source the stresses are of compression until the return of the source of heat. After the passage of the source, the stresses begin to increase up to the material flow stress.

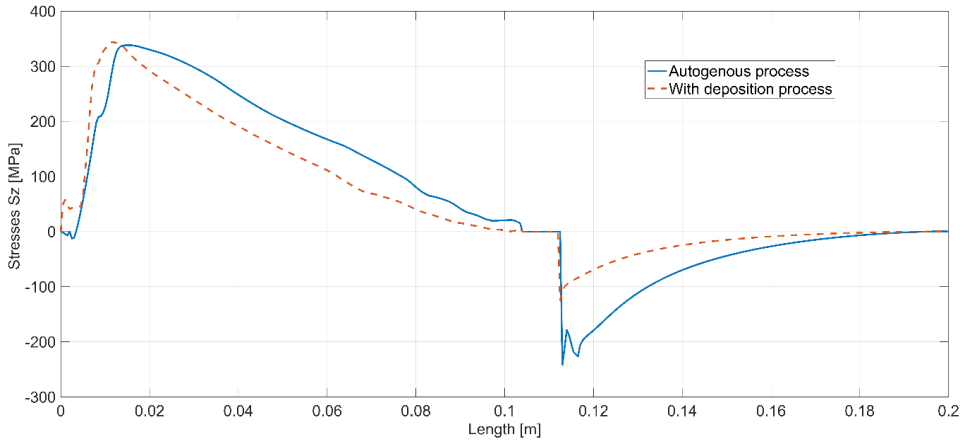

Figure 18 – Longitudinal stresses Sz for t=20 s

4. REFERENCES

Tsirkas, S.,A. ; Papanikos, P.; Pericleous, K.; Strusevich, N.; Boitot, F.; Bergheau, J. M. Evaluation of distortions in laser welded shipbuilding parts using local – global finite element approach. Science and Technology of Welding and Joining 2003 Vol. 8 No. 2.

Deng, D., Murakawa, H. Prediction of welding distortion and residual stress in a thin plate butt-welded joint. Computational Materials Science.

Miettinen, J. Calculation of Solidification-Related Thermophysical Properties for Steels. Metallurgical and Materials Transactions B (1997) V.28, p.281-297.

5. RESPONSIBILITY NOTICE

The author(s) is (are) the only responsible for the printed material included in this paper.